Progress In Electromagnetics Research B, Vol. 76, 141–157, 2017

Scattering and Radiation Characteristics of Antenna Systems under Nose Dielectric Radomes

Oleg Sukharevsky, Vitaly Vasylets*, and Sergey Nechitaylo

Abstract—The calculation method for electromagnetic field scattered by antenna placed inside nose dielectric radome is proposed. To obtain the radiation characteristics we use the calculation method for field generated by radiation aperture given that an arbitrary system of scatterers (particularly, radome) exists in its vicinity. Also the method for calculating radiation characteristics of antenna system with the same radomes is obtained. Considered numerical results tell us that influence of radome on radiation characteristics can be reduced to minimum for any radome type. Besides, the radome can reduce the radar visibility of antenna system outside of its operating frequency range.

1. INTRODUCTION

The majority of airborne targets (for example, aircrafts, and missiles with homing heads) have nose radomes that cover antenna system (Fig. 1). Existing antenna systems can significantly increase the radar cross section (RCS) of entire radar object [1].

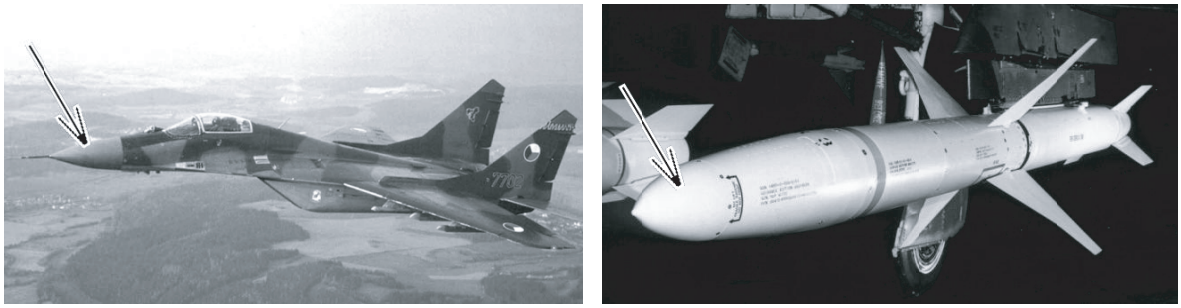

(a) (b)

Figure 1. Use of antenna systems under dielectric radomes by (a) aircrafts and (b) missiles.

So, development of the calculation method for evaluating scattering characteristics (specifically, RCS) of antenna systems under radomes is a very important problem to be solved while designing detection algorithms for airborne targets. Internal system interactions appearing once the "antenna-radome" system gets illuminated lead to highly complicated calculation algorithms. Geometrical-optics methods usually used for calculating scattering characteristics for such system [2, 3] do not account for these interactions (multiple reflections between antenna and radome). At the same time, electrodynamic interaction between antenna reflector and the radome can lead to significant increase (often, with

Received 22 March 2017, Accepted 8 June 2017, Scheduled 27 June 2017

* Corresponding author: Vitaly Vasylets (admin@radar.dinos.net).
The authors are with the Kharkiv Kozhedub University of Air Forces, Kharkiv, Ukraine.

resonant behavior) in antenna system RCS [4], and, consequently, in the RCS of entire radar object. Iterative method proposed in [5] for "antenna-radome" system was developed under the following limitations: firstly, all considerations were given for two-dimensional models; secondly, the radome shape had to have very small curvatures. In [4], the bounded dielectric plate was used instead radome. Thus, it is necessary to develop asymptotic method for calculating RCS of reflector antenna system with nose dielectric radome in three-dimensional configuration. Such method would need to account for at least first order re-reflections between the antenna and radome.

Some computational models have been described in recent papers for performance of radiation patterns of radar antennas with dielectric radomes [6–13]. But the publications known to us do not contain results concerning the RCS of antennas under nose radomes (problem 1 in our paper).

In addition to calculating the scattering characteristics (problem 1), it is necessary to also calculate directivity pattern of such antenna system (problem 2). From the viewpoint of manufacturer, the manufacturability is very important in radome making. Therefore, three kinds of radomes are considered in the paper: ogival, compound cone (consisting of several truncated cones) and, in addition, pyramidal (with regular octagon as base). Both scattering characteristics and directivity pattern are obtained for these radome kinds. Solving methods for the two problems (1 and 2) are based on using the same "key" problems. In addition, general approach to calculations regarding the "antenna-radome" system is the same for different radome kinds. Some computation details (if necessary) will be described along with the results.

In the beginning, we consider antenna system under the nose radome, which is conjugation (not smooth) of truncated cones (Fig. 2). The relative permeability of cones' material is $\varepsilon' = 3.8 + j0.0076$. Inside the radome, there is a phased-array antenna with octagonal aperture (Fig. 1). As a first approximation, we assume the antenna to be represented by an octagonal plate and the field scattered by the antenna itself (as it is done usually in engineering) will be multiplied by factor of ≈ 0.9. Such representation provides satisfactory approximation to the field scattered by antenna surface (if the wavelength of sounding wave is much greater than that the antenna operation wavelength). In nose part of radome, there is metallic spherical cap conjugated smoothly with the top truncated cone (Fig. 2). The presence of this cap is accounted for in electromagnetic calculations by beam tracing method. The later means that wave passing through the radome (in geometrical optics approximation) is altered as follows: the incident beam hitting the metallic cap surface doesn't pass to the radome inside. The field scattered by the radome itself accounts for the scattering by metallic half spherical cap.

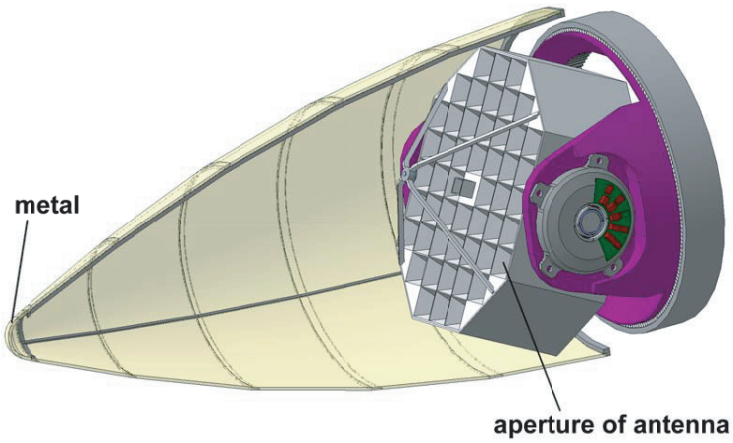

Figure 2. General appearance of antenna under compound dielectric radome.

Considering all the above, the "key" problem is calculation of scattering by the side surface of cone radome with octagonal plate placed inside it (accounting for the reflection coefficient multiplied by factor of 0.9).

Moreover, the method proposed here accounts for the influence of beams that pass through radome and do not hit the antenna aperture directly but rather get rescattered by the radome's inner surface.

It should be noted that the same beam can pass through radome at a surface point belonging to one truncated cone but it can rescatter from the inner surface belonging to another one.

Below, we consider solution procedure for the "key" problem stated above [16].

2. ELECTROMAGNETIC WAVE SCATTERING BY ANTENNA SYSTEM UNDER THE NOSE DIELECTRIC RADOME

In this section, we consider the scattering from antenna under different types of radomes.

2.1. Electromagnetic Wave Scattering by Antenna System under the Cone Dielectric Radome

We consider plane electromagnetic wave

$$\begin{aligned}\vec{E}^0(\vec{x}) &= \vec{p}^0 \exp\left(jk_0\left(\vec{R}^0\cdot\vec{x}\right)\right),\\ \vec{H}^0(\vec{x}) &= \sqrt{\frac{\varepsilon_0}{\mu_0}}\left(\vec{R}^0\times\vec{p}^0\right)\exp\left(jk_0\left(\vec{R}^0\cdot\vec{x}\right)\right),\end{aligned} \tag{1}$$

which is incident from without upon the model of reflector antenna system under the cone radome (Fig. 3).

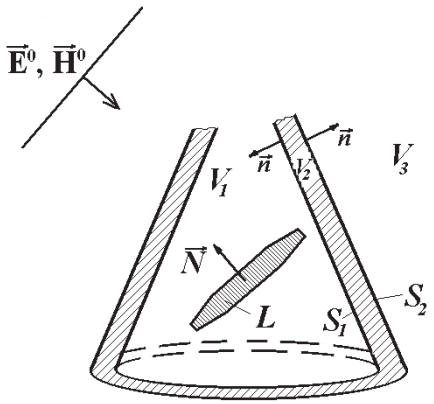

Figure 3. The "antenna-radome" system.

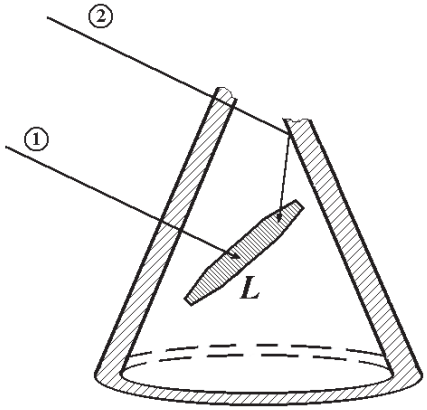

Figure 4. Propagation paths of incident wave.

Application of the Lorentz reciprocity theorem to the sought total field ($\vec{E}$, $\vec{H}$) and to auxiliary field ($\vec{\hat{E}}$, $\vec{\hat{H}}(\vec{x}|\vec{x}_0,\vec{p})$), the latter corresponding to that of electric dipole placed at point $\vec{x}_0$ that has the vector-moment $\vec{x}_0 = -r\vec{R}^0$ given that only radome is present, allows us to obtain integral representation of the field we seek [16]:

$$j\omega\vec{p}\cdot\vec{E}(\vec{x}_0) = j\omega\vec{p}\cdot\vec{E}^{scat.}_{radome}(\vec{x}_0) + \int\limits_L \left(\vec{K}(\vec{x})\cdot\vec{\hat{E}}^T(\vec{x}|\,\vec{x}_0,\vec{p})\right)\mathrm{d}S, \tag{2}$$

where $\vec{E}^{scat.}_{radome}(\vec{x}_0)$ is the field scattered by the radome only, and $\vec{K}(x)$ is the surface current density over the antenna reflector's surface. Integral summand of Expression (2) represents the response of antenna reflector onto incident wave that takes into account electromagnetic wave interaction with the radome. Having assumed $\vec{x}_0 = -r\vec{R}^0$ and further assumed that $r\to\infty$, we receive expression for resulted field scattered from the "antenna-radome" system in the far-field zone:

$$\vec{p}\cdot\vec{E}(\vec{R}^0) \sim \vec{p}\cdot\vec{E}^{scat.}_{radome}\left(\vec{R}^0\right) - jk_0\frac{e^{jk_0r}}{4\pi r}\sqrt{\frac{\mu_0}{\varepsilon_0}}\int\limits_L\left(\vec{\hat{E}}(\vec{x})\cdot\vec{K}(\vec{x})\right)\mathrm{d}S. \tag{3}$$

Here, $\vec{\hat{E}}(\vec{x})$ is the field excited by primary incident plane wave in Eq. (1) at points of the reflector's surface L given that only radome is present. We are going to compute this field by method of geometrical optics.

Under approximation assumed above, we represent $(\vec{\hat{E}}(\vec{x}),\ \vec{\hat{H}}(\vec{x}))$ as a sum of field that passes to reflector directly through the illuminated part of radome (propagation path 1 in Fig. 4) and the field that passes to reflector via single reflection from the inner wall of radome (propagation path 2 in Fig. 4).

The field corresponding to propagation path 1 in Fig. 4 can be presented as:

$$\vec{\hat{E}}_1(\vec{x}) = \left[\tau_\perp p_\perp \vec{e}_\perp + \tau_\parallel p_\parallel \left(\vec{R}^0 \times \vec{e}_\perp\right)\right] \exp\left(jk_0\left(\vec{R}^0 \cdot \vec{x}\right)\right), \tag{4}$$

$$\vec{\hat{H}}_1(\vec{x}) = \sqrt{\frac{\varepsilon_0}{\mu_0}}\left[\tau_\perp p_\perp \left(\vec{R}^0 \times \vec{e}_\perp\right) - \tau_\parallel p_\parallel \vec{e}_\perp\right] \exp\left(jk_0\left(\vec{R}^0 \cdot \vec{x}\right)\right), \tag{5}$$

where $\vec{e}_\perp = \frac{\vec{R}^0 \times \vec{n}}{|\vec{R}^0 \times \vec{n}|}$, $\vec{e}_\parallel = (\vec{R}^0 \times \vec{e}_\perp)$, $p_\perp = (\vec{p} \cdot \vec{e}_\perp)$, $p_\parallel = (\vec{p} \cdot \vec{e}_\parallel)$, and $\vec{n}$ is the vector of the normal to the radome surface.

Complex valued coefficients $\tau_\perp$, $\tau_\parallel$ describe propagation of plane electromagnetic wave through flat uniform layer with the properties of radome at two mutually orthogonal polarizations. As parallel polarization marked by sign $\parallel$, we consider the situation where electric field intensity vector of incident wave belongs to the plane passing through vector $\vec{R}^0$ and normal $\vec{n}$ at every particular point of the radome surface. Accordingly, the perpendicular polarization, marked by sign $\perp$, corresponds to situation where electric field intensity vector is orthogonal to the plane specified above. General expression for the propagation coefficient can be presented as follows

$$\tau = \left(\left(\cos\kappa\delta + \frac{j}{c}\sin\kappa\delta\right) + \left(\cos\kappa\delta - \frac{j}{c}\sin\kappa\delta\right)\rho\right)\exp\left(-jk_0\delta\cos\theta\right), \tag{6}$$

where ρ is the complex valued coefficient of reflection from plain uniform layer of material that has the properties of radome. This coefficient can be expressed as:

$$\rho = \frac{j\left(c^2-1\right)\sin\kappa\delta}{2c\cos\kappa\delta - j\left(c^2+1\right)\sin\kappa\delta}. \tag{7}$$

Here $c = \frac{\sqrt{\varepsilon' - \sin^2\theta}}{\beta\cos\theta}$, $\kappa = k_0\sqrt{\varepsilon' - \sin^2\theta}$, $\cos\theta = |(\vec{R}^0 \cdot \vec{n})|$, $\sin^2\theta = 1 - (\vec{R}^0 \cdot \vec{n})^2$, ε' is relative permittivity of the radome material, and δ is the radome thickness.

$$\beta = \begin{cases} 1 \text{ in case } \perp \text{ polarization,} \\ \varepsilon' \text{ in case } \parallel \text{ polarization.} \end{cases}$$

In the case of polarization $\perp$, we have $\rho = \rho_\perp$, $\tau = \tau_\perp$, and in the case of polarization $\parallel$, we have $\rho = \rho_\parallel$, $\tau = \tau_\parallel$.

If the ray passing through radome at some point $\vec{x}_0$ does not hit the reflector, then it must pass through radome once again at some point $\vec{x}_1$ at the "shadow" part of radome surface. Taking into account that the equation of cone surface has the following form:

$$\begin{gathered} x = z\tan\theta\cos s, \\ y = z\tan\theta\sin s, \\ (0 \le z \le h,\ 0 \le s \le 2\pi), \end{gathered} \tag{8}$$

and using equation of beam in parametric form

$$\begin{aligned} x &= x_0 + R_1^0 t, \\ y &= y_0 + R_2^0 t, \\ z &= z_0 + R_3^0 t, \end{aligned} \tag{9}$$

where (x_0, y_0, z_0) is a point at the "illuminated" surface of cone, and we obtain the value t_1, which corresponds to point $\vec{x}_1$ at the "shadow" part of radome surface:

$$t_1 = 2\frac{R_3^0 z_0 \tan^2\theta - R_1^0 x_0 - R_2^0 y_0}{1 - R_3^{0^2}/\cos^2\theta}. \tag{10}$$

If we find, in this case, the values for $\tau_\perp$, $\tau_\parallel$, $\rho_\perp$, $\rho_\parallel$, $\vec{e}_\perp$, $\vec{e}_\parallel$ at point $\vec{x}_0$, then we can compute the intensity vector of electric field that has propagated through radome at point $\vec{x}_0$ and that is incident onto its inner surface at point $\vec{x}_1$

$$\vec{p}_1 \exp\left(jk_0\left(\vec{R}^0 \cdot \vec{x}_1\right)\right), \quad \vec{p}_1 = \tau_\perp p_\perp \vec{e}_\perp + \tau_\parallel p_\parallel \vec{e}_\parallel. \tag{11}$$

Vector $\vec{p}_1$, wave incidence direction $\vec{R}_0$, and the normal $\vec{n}\,(\vec{x}_1)$ to inner surface of radome S_1 at point $\vec{x}_1$ can be used for finding $\tau_{1\perp}$, $\tau_{1\parallel}$, $\rho_{1\perp}$, $\rho_{1\parallel}$, $\vec{e}_{1\perp}$, $\vec{e}_{1\parallel}$ by means of formulas (6) and (7). The field that has reflected from inner surface of radome at point $\vec{x}_1$ and that is incident onto antenna's reflector (path 2 in Fig. 4) can be represented as follows:

$$\vec{\hat{E}}_2(\vec{x}) = \left[\rho_{1\perp} p_{1\perp} \vec{e}_{1\perp} + \rho_{1\parallel} p_{1\parallel}\left(\vec{R}^1 \times \vec{e}_{1\perp}\right)\right] \exp\left(jk_0\left[\left(\vec{R}^0 \cdot \vec{x}_1\right) + \left(\vec{R}^1 \cdot \vec{x}\right)\right]\right), \tag{12}$$

$$\vec{\hat{H}}_2(\vec{x}) = \sqrt{\frac{\varepsilon_0}{\mu_0}}\left[-\rho_{1\parallel}\, p_{1\parallel} \vec{e}_{1\perp} + \rho_{1\perp} p_{1\perp}\left(\vec{R}^1 \times \vec{e}_{1\perp}\right)\right] \exp\left(jk_0\left[\left(\vec{R}^0 \cdot \vec{x}_1\right) + \left(\vec{R}^1 \cdot \vec{x}\right)\right]\right), \tag{13}$$

where $\vec{R}^1 = \vec{R}^0 - 2\vec{n}(\vec{x}_1)(\vec{R}^0 \cdot \vec{n}(\vec{x}_1))$.

It should be noted that once plane electromagnetic wave bounces off the inner surface of radome, caustic surface may form. Computation of such caustic surface that appears in the case of oblique incidence of plane wave onto the radome cone has been carried out in [16]. The ray passing through such caustic surface changes its phase by $\pi/2$ [14, 15], which has to be taken into account for the wave hitting the antenna after reflection from the radome inner surface.

Surface current density $\vec{K}(\vec{x})$ over antenna reflector in expression (3) is computed in form of sum of currents excited on the reflector's surface by "direct" and "reflected" waves (path 1 and path 2 in Fig. 4). In the physical optics approximation, current surface density can be expressed as

$$\vec{K}\,(\vec{x}) = 2\left(\vec{N} \times \vec{\hat{H}}\right), \tag{14}$$

where $\vec{N}$ is the vector of normal to the reflector's surface at point $\vec{x}$, and $\vec{\hat{H}}$ can be computed as a sum of magnetic field intensities for the first and second paths of incident wave propagation according to expressions (5) and (13) respectively.

In our case, the vector of normal $\vec{N}$ is constant, and incidence of direct and reflected beam to octagonal antenna aperture can be calculated as follows.

Let the plane containing antenna aperture (Fig. 5) be described by equation

$$-x\sin\alpha - z\cos\alpha = \mathrm{d}, \tag{15}$$

and the incident wave direction be described by unit vector $\vec{R}^0 = (R_1^0, R_2^0, R_3^0)$.

The direct (reflected) beam can be expressed in parametric form Eq. (9).

We find the crossing point for beam and plane (15):

$$\begin{aligned} x* &= x_0 + R_1^0 t_0, \\ y* &= y_0 + R_2^0 t_0, \\ z* &= z_0 + R_3^0 t_0, \end{aligned}$$

where

$$t_0 = -\frac{x_0 sin\alpha + z_0\cos\alpha + d}{R_1^0 sin\alpha + R_3^0\cos\alpha}.$$

Next, we switch to local coordinate system (x', y', z'), which results from rotation of coordinate system (x, y, z) by angle α in plane (xOz):

$$\begin{cases} x' = x\cos\alpha - z\sin\alpha \\ y' = y \\ z' = x\sin\alpha + z\cos\alpha + d \end{cases}$$

Fig. 6 shows appearance of the octagonal aperture L.

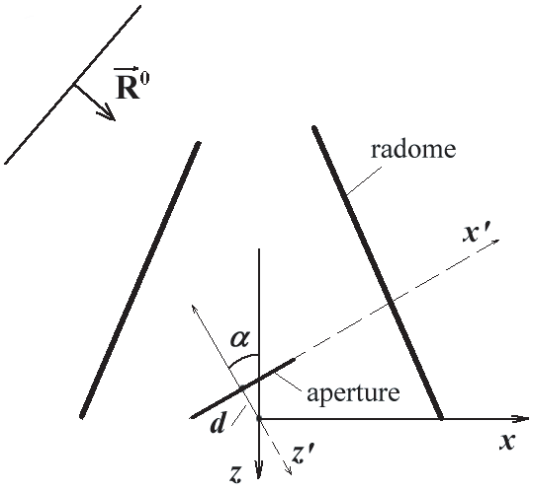

Figure 5. Geometry of the antenna aperture relative position inside the radome.

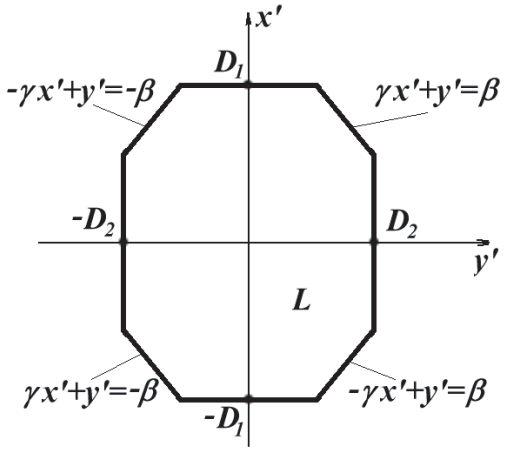

Figure 6. The geometry of octagonal aperture.

We find the crossing point of beam and aperture in plane $(x'Oy')$:

$$\begin{aligned} x' &= x^* \cos\alpha - z^* \sin\alpha, \\ y' &= y^*. \end{aligned} \tag{16}$$

Then, the region L can be described by the system of inequalities:

$$L: \ \left|x'\right| \le D_1; \quad \left|y'\right| \le D_2; \quad \left|\gamma x' + y'\right| \le \beta; \quad \left|-\gamma x' + y'\right| \le \beta. \tag{17}$$

Thus, if conditions in Eqs. (16) and (17) are met, then we can conclude that the beam crosses the octagonal antenna aperture.

The field $\vec{p}\cdot\vec{E}^{scat}_{radome}(\vec{R}^0)$ scattered by radome can be computed using Kirchhoff's approximation [16]:

$$\vec{p}\cdot\vec{E}^{scat}_{radome}\left(\vec{R}^0\right) \approx -jk_0\frac{e^{jk_0r}}{4\pi r}\times\iint\limits_{S_{illum.}}\left[\left(\vec{p}\cdot\left(\vec{n}\times\vec{H}'\left(\vec{x}\right)\right)\right)\sqrt{\frac{\mu_0}{\varepsilon_0}}+\vec{E}'\left(\vec{x}\right)\cdot\left(\vec{n}\times\left(\vec{p}\times\vec{R}^0\right)\right)\right]\times \exp\left(jk_0\left(\vec{R}^0\cdot\vec{x}\right)\right)dS. \tag{18}$$

Here, $(\vec{E}', \vec{H}')$ is the field at (or close to) illuminated surface of radome, which, in the Kirchhoff's approximation, can be expressed as

$$\vec{E}'(\vec{x}) \approx \left[\rho_\perp(\vec{x})p_\perp(\vec{x})\frac{\left(\vec{R}^1\times\vec{n}\right)}{\left|\vec{R}^1\times\vec{n}\right|}+\rho_\parallel(\vec{x})p_\parallel(\vec{x})\frac{\vec{R}^1\times\left(\vec{R}^1\times\vec{n}\right)}{\left|\vec{R}^1\times\left(\vec{R}^1\times\vec{n}\right)\right|}\right]\exp\left(jk_0\left(\vec{R}^1\cdot\vec{x}\right)\right), \tag{19}$$

$$\vec{H}'(\vec{x}) = \frac{1}{j\omega\mu_0}\vec{\nabla}\times\vec{E}'(\vec{x}), \tag{20}$$

where $\vec{R}^1 = \vec{R}^0 - 2\vec{n}(\vec{R}^0\cdot\vec{n})$, and $\vec{n} = \vec{n}(x)$ is the normal to the outer radome surface S_2. For dielectric radome of conical shape, representation in Eq. (18) can be simplified and reduced to single integral by angular coordinate α tied to the illuminated part of radome:

$$\vec{p}\cdot\vec{E}^{scat.}_{radome}\left(\vec{R}^0\right) \approx -jk_0\frac{e^{jk_0r}}{4\pi r}\frac{\sin\theta}{\cos^2\theta}\int\limits_{\alpha_0}^{\alpha_1}\Psi\left(\alpha\right)\,d\alpha, \tag{21}$$

where

$$\begin{aligned}
\Psi(\alpha) &= F(\alpha)\left[\frac{h\exp(j2k_0h\varphi(\alpha))}{2jk_0\varphi(\alpha)}+\frac{\exp(j2k_0h\varphi(\alpha))-1}{4k_0^2\varphi^2(\alpha)}\right],\\
F(\alpha) &= \left(\rho_\perp(\alpha)p_\perp^2(\alpha)-\rho_\parallel(\alpha)p_\parallel^2(\alpha)\right)\left(\vec{R}^0\cdot\vec{n}(\alpha)\right),\\
\varphi(\alpha) &= \mathrm{tg}\theta\left(R_1^0\cos\alpha+R_2^0\sin\alpha\right)+R_3^0,\\
\alpha_0 &= \mathrm{arcctg}\frac{\eta}{\sqrt{1-\eta^2}},\quad \alpha_1=2\pi-\alpha_0,\quad \eta=\frac{\mathrm{tg}\theta}{\mathrm{tg}\gamma},
\end{aligned}$$

h is the radome height, θ the half-aperture angle of the cone, γ the angle between the cone axis and the vector $\vec{R}^0$, and $\vec{n}(\alpha)$ the vector of normal to outer surface of radome S_2.

2.2. Some Calculation Peculiarities for Radomes with Ogival and Pyramidal Shape

To do the calculations for ogival shaped radome, it is necessary to know the exact shape of the radome surface and the normal unit vector at every surface point. In other respects, the calculations for ogival radome are similar to those for the cone radome.

The ogival shape can be set by function

$$z-c=a\left(d-\sqrt{x^2+y^2}\right)^\alpha, \tag{22}$$

where parameters a, c, α, d are set so that surface of ogival radome follows as close as possible the surface of compound cone radome (passes through conjunction lines of compound cone). In our case, these parameters were as follows: $a=-1.579, c=0.054\,\mathrm{m}$, $\alpha=0.5593$, $d=0.12\,\mathrm{m}$. The normal unit vector to the side surface of the ogival radome has the form:

$$\begin{aligned}
&\vec{N}=(F_x,F_y,F_z)\Big/\sqrt{F_x^2+F_y^2+F_z^2},\\
&F_x=a\alpha\left(d-\sqrt{x^2+y^2}\right)^{\alpha-1}\cdot\frac{x}{\sqrt{x^2+y^2}},\\
&F_y=a\alpha\left(d-\sqrt{x^2+y^2}\right)^{\alpha-1}\cdot\frac{y}{\sqrt{x^2+y^2}},\\
&F_z=1.
\end{aligned} \tag{23}$$

Crossing point between the incident wave beam with the inner ("shadow") part of ogival surface is found similarly to the cone surface, but instead of getting quadratic equation for finding parameter t_1 (such as Eq. (10)) we obtain, generally speaking, non-algebraic equation, which can be solved using bisection (Bolzano) method [17].

When doing calculations for the system with pyramidal radome, the radome model was designed as follows. The N-gon is used as a base of pyramid. In our calculation, we used $N=8$. The origin of coordinate system coincided with the polygon center. The radius-vector of the pyramid vertex is $\vec{r}_0=(0,0,H)$. The radius-vectors of polygon apices are $\vec{r}_i=(x_i,y_i,z_i)$, $(i=1,\ldots,N)$. Here, $x_i=\rho_0\cos\varphi_i$; $y_i=\rho_0\sin\varphi_i$; $z_i=0$, $\varphi_i=\alpha+\frac{2\pi}{N}(i-1)$, $\varphi_{N+1}\equiv\varphi_1$; and ρ_0 is the radius of circle circumscribing the N-gon. In this case, the unit normal vector to i-th side has the form:

$$\vec{n}_i=\frac{((\vec{r}_0-\vec{r}_i)\times(\vec{r}_0-\vec{r}_{i+1}))}{|(\vec{r}_0-\vec{r}_i)\times(\vec{r}_0-\vec{r}_{i+1})|}, \tag{24}$$

and equation for the i-th side plane is:

$$\vec{n}_i(\vec{r}_0-\vec{r}_i)=0. \tag{25}$$

If incident plane wave propagates in direction $\vec{R}_0$, then the side is checked for being "illuminated" or not by the sign of $(\vec{R}_0\cdot\vec{n})$.

Simple calculation allows to write the surface integral for the illuminated pyramid side $\Sigma(\varphi_i < \varphi < \varphi_{i+1})$:

$$\iint\limits_{\Sigma} f(x,y,z)\,ds = \frac{1}{\cos\beta}\int\limits_{\varphi_i}^{\varphi_{i+1}} d\varphi \int\limits_{0}^{\rho_1(\varphi)} f(x,y,z)\,\rho d\rho. \tag{26}$$

The integral of Eq. (26) type is used for obtaining the field scattered by pyramid side. Parameters of the function f depend on ρ,φ as follows:

$$x = \rho\cos\varphi; \quad y = \rho\sin\varphi; \quad z = \frac{\rho_1(\varphi)-\rho}{\rho_1(\varphi)}\cdot H, \quad \text{and} \quad \beta = \operatorname{arctg}\left(H/(\rho_0\cos(\pi/N))\right). \tag{27}$$

Also, we can find the crossing point of the beam propagating in direction $\vec{R}_0$ and passing through "illuminated" side and the "shadow" side. Let's assume that we check the j-th "shadow" side. Then, the radius-vector of crossing point at the j-th side is

$$\vec{r}* = \vec{r}_0 + \vec{R}^0\frac{\vec{n}_j\cdot(\vec{r}_j-\vec{r}_0)}{\left(\vec{R}^0\cdot\vec{n}_j\right)}, \tag{28}$$

where $\vec{r}_0$ is the radius-vector of crossing point at the "illuminated" side that the beam passed through.

2.3. Results of the Scattering Characteristics Calculation for Antenna System under the Nose Dielectric Radome

The scattering characteristics calculations for compound cone, ogival, and pyramidal radomes were carried out and possible differences in scattered filed were estimated for each kind of radome. When computing the field radiated by the antenna, we evaluated directivity patterns for the antenna under the same radome kinds (similar to computations presented in Section 3.2).

Our computation model was the antenna system with the following parameters. The total radome height was $h = 454$ mm, the radius of metallic spherical cap at the radome peak was 18 mm, The radius of radome base (the radius of circle circumscribing the base of pyramidal radome) is 120 mm. Dielectric part of compound radome consisted of 5 truncated cones (Fig. 2) with the height of 75–90 mm and the half-aperture angles (angle between the cone axis and the cone generatrix) of 22.1, 19, 13.4, 8.8, and 4 degrees. The side surface of ogival radome followed as close as possible the shape of compound cone radome (passed through conjunction lines of compound cone). The equation for side surface of ogival radome in Eq. (22) was presented in Section 2.2. Octahedral pyramidal radome was inscribed into circular cone of the same height.

Relative permeability of the radome material was $\varepsilon' = 3.8 + j0.0076$. The distance between radome base and antenna aperture's center of rotation was 54 mm (Fig. 2), the distance from aperture center of rotation to aperture plane was 40 mm (Fig. 5), the length of octagonal antenna aperture along axis x' (Fig. 6) was 188 mm, width of the aperture along axis y' was 145 mm, parameters γ, β for expression (17) were equal to 0.96511 and 0.12172 respectively. The wavelength of illumination signal was 30 mm (frequency was 10 GHz). The antenna was turned in plane Oxz by angle 15 degrees with respect to the radome axis.

In Section 3, the optimal (regarding the transmission coefficient) thicknesses of radome walls will be calculated for antenna operating frequency of 36.6 GHz, it takes the values of 2.4 and 4.75 mm. For these thickness values, the dependencies of RCS versus the elevation angle of illumination direction are presented in Figs. 7–10 for the three radome kinds and two polarizations of illumination signal. Every plot shows 2 dependencies for pyramidal radome: pyramid 1 — illumination direction vector $\vec{R}_0$ belongs to the plane perpendicular to one of the pyramid sides; pyramid 2 — illumination direction vector $\vec{R}_0$ belongs to a bisector plane between two radome sides.

Dependencies in Figs. 7–10 show that antenna aperture RCS given absent radome was equal to 6.60 m^2 in case of orthogonal incidence of illumination signal to it. The use of radomes of the 2.4 and 4.75 mm thicknesses reduces this maximum to 2–3 m^2 for parallel polarization of illumination signal and to 2–4 m^2 for perpendicular polarization of illumination signal. The RCS maximum level for pyramidal

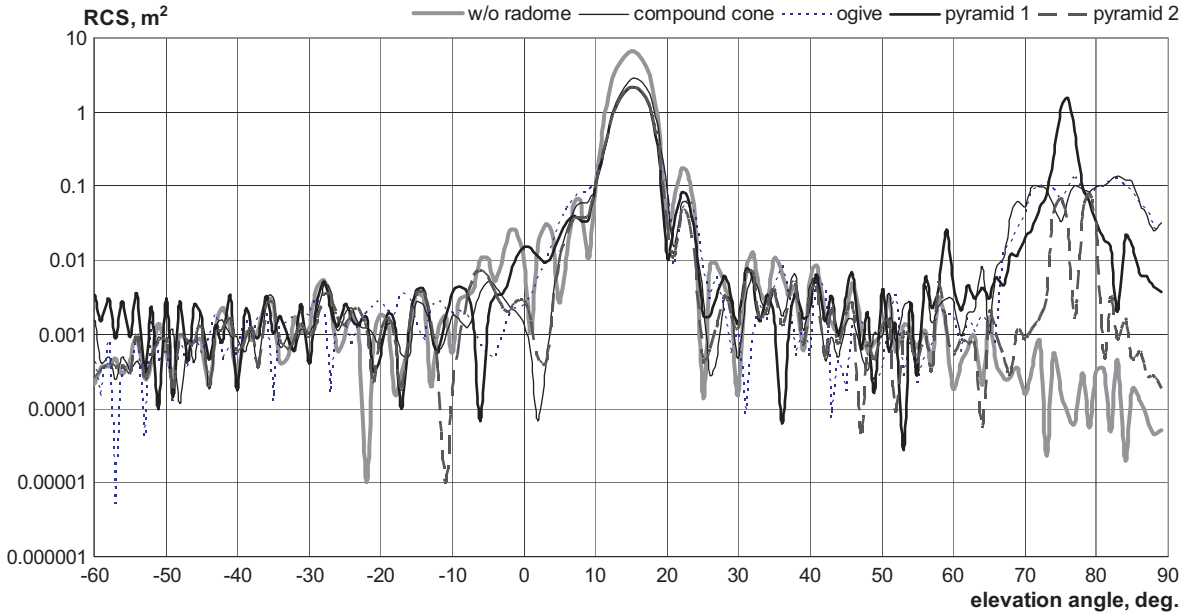

Figure 7. RCS of antenna system versus elevation angle for perpendicular polarization given radome thickness of 2.4 mm.

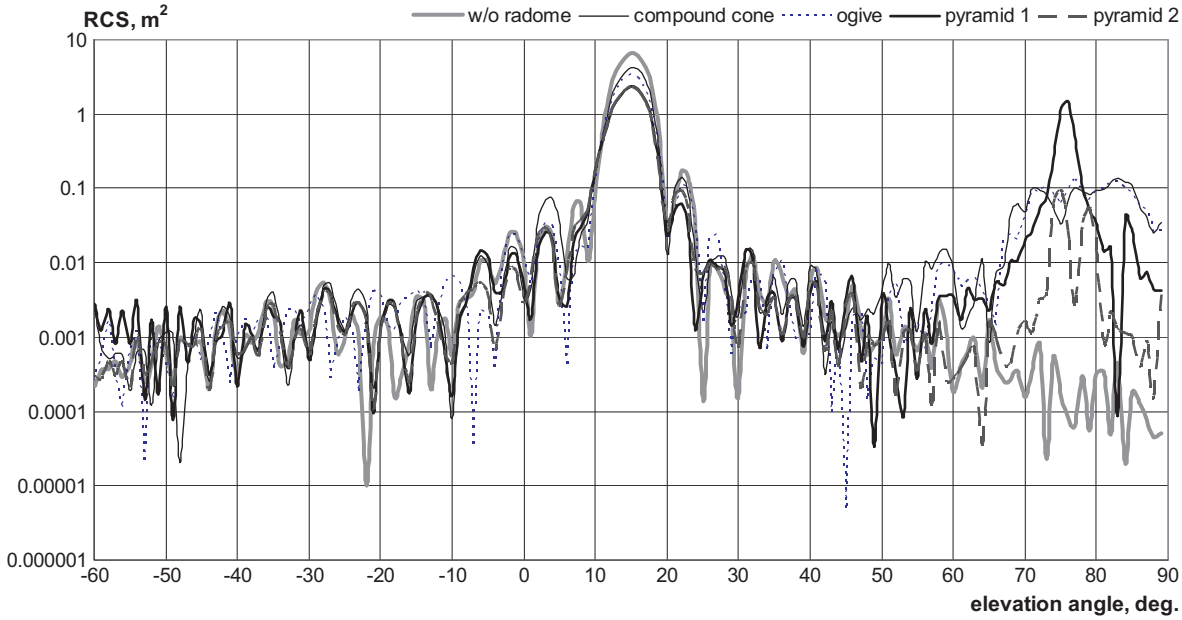

Figure 8. RCS of antenna system versus elevation angle for parallel polarization given radome thickness of 2.4 mm.

radome is slightly lower than for compound cone and ogival radomes. Contribution of metallic cap into the total antenna system RCS was very small ($\sim 0.001\,\mathrm{m}^2$), and its influence on the general scattering level is negligible.

Reflections from the radome provide significant contributions into RCS given small values of elevation angles as well as given elevation angle of 70 degrees, which corresponds to the wave incidence perpendicularly to the cone radome generatrix. The side surface of compound or ogive radome is close to cone surface. At the same time the scattering from such radomes is essential for illumination directions

close to normal vector for that cone surface.

In a similar way for pyramidal radome the RCS peaks will arise for illumination directions orthogonal to radome sides or edges. For pyramidal radome, the contribution of its side surface to total RCS can be as high as 1.8 m^2 but this only occurs given the elevation angle of 76 degrees and only for the case where the illumination direction vector $\vec{R}_0$ is perpendicular to one of the pyramid sides. In the latter case, the lobe width is less than 3 degrees.

Contribution of reflections from the "shadow" part to the total scattered field is quite small for

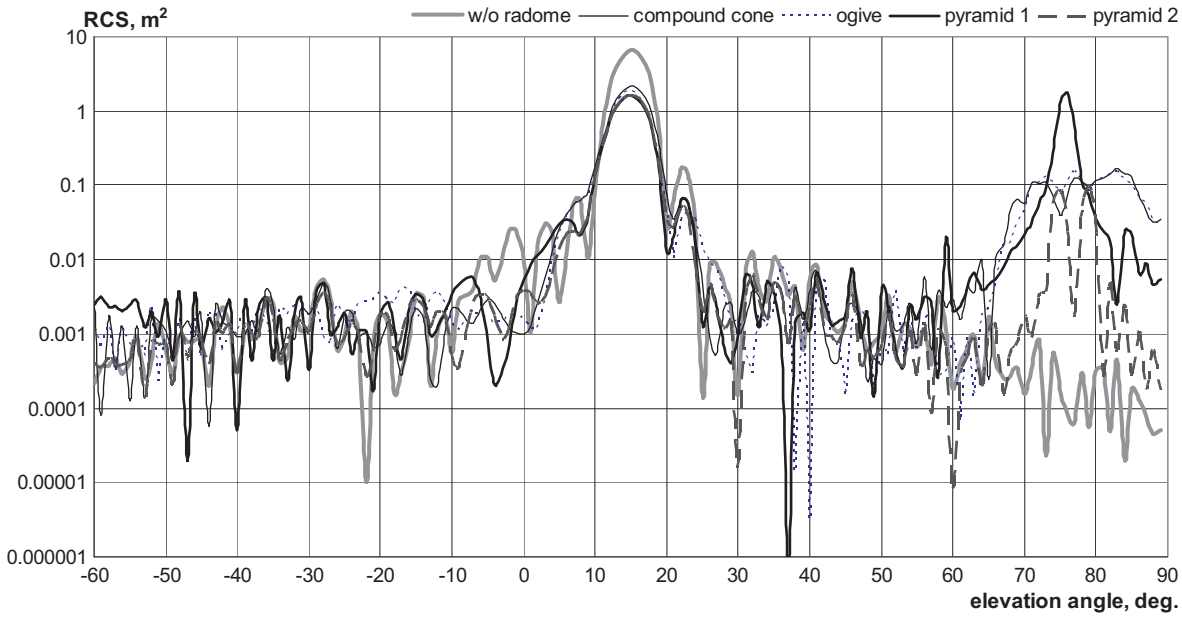

Figure 9. RCS of antenna system versus elevation angle for perpendicular polarization given radome thickness of 4.75 mm.

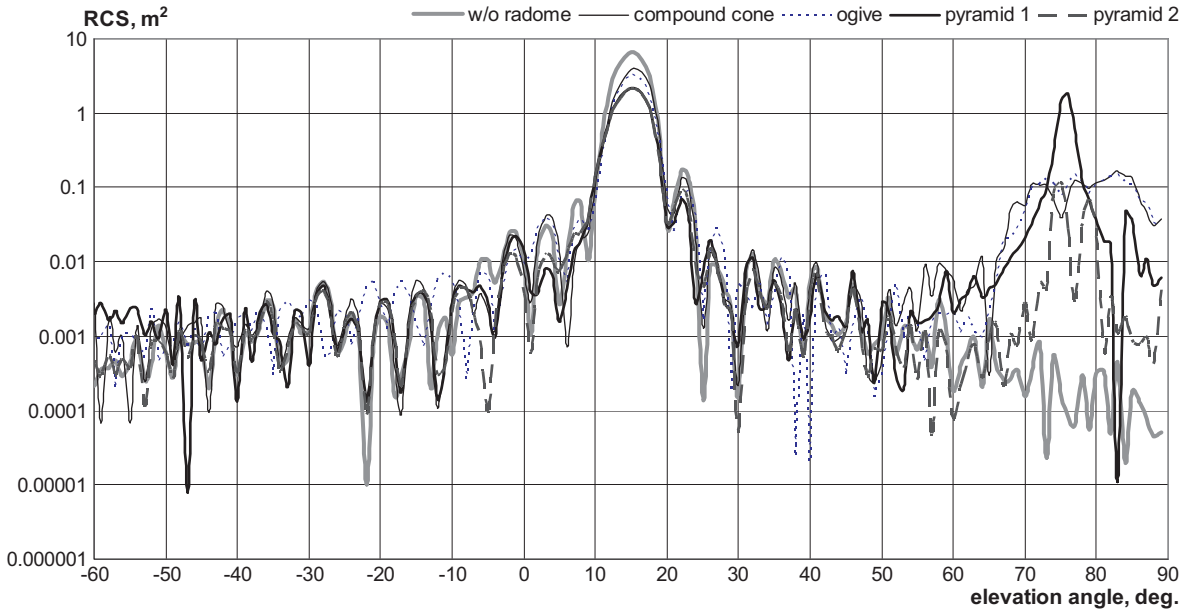

Figure 10. RCS of antenna system versus elevation angle for parallel polarization given radome thickness of 4.75 mm.

majority of illumination directions and it amounts to hundredth of square meter for elevation angle of 58–60 degrees only in two cases: parallel polarization for compound cone radome and perpendicular polarization for pyramid when illumination direction vector $\vec{R}_0$ lies in the plane perpendicular to this "shadow" side of pyramid.

The width of main lobe of antenna system scattering diagram is less than a few degrees; besides, the strong scattering is concentrated near direction that is perpendicular to antenna aperture. For majority of illumination aspect angles the RCS of the considered antenna system is less than $0.1\,\mathrm{m}^2$ for any radome kind.

3. RADIATION OF ANTENNA SYSTEM UNDER THE NOSE DIELECTRIC RADOME

In this section, we consider the radiation properties of antenna under radome, the design of which was described in the previous section.

3.1. Method for Calculating the Radiation of the Antenna under Radome

Let antenna be an octagonal aperture S_0 (Fig. 11) cut in perfectly absorbing plane.

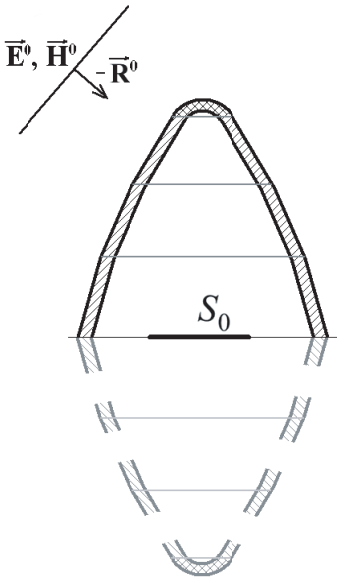

Figure 11. "Simmetrized" radome.

Then, as it was shown in [16], the field radiated by that antenna system in direction $\vec{R}^0$ can be represented by formula

$$\vec{p}\cdot\vec{E}\left(\vec{R}^0\right)=\int\limits_{S_0}\left(\left(\vec{E}^T(x)\times\vec{H}_0\left(x,\vec{R}^0,\vec{p}\right)\right)-\left(\vec{H}^T(x)\times\vec{E}_0\left(x,\vec{R}^0,\vec{p}\right)\right)\right)\cdot d\vec{S}. \tag{29}$$

Here $\vec{E}_0(x,\vec{R}^0,\vec{p})$, $\vec{H}_0(x,\vec{R}^0,\vec{p})$ is the field scattered by "symmetrized" radome (Fig. 11) at the aperture points x (at which the perfectly absorbing screen is absent). This field is generated by incident plane wave with the direction unit vector $(-\vec{R}^0)$, or

$$\begin{aligned}\vec{E}_0 &= \left(\vec{R}^0\times\left(\vec{p}\times\vec{R}^0\right)\right)\exp\left(-jk_0\left(\vec{R}^0\cdot\vec{x}\right)\right),\\ \vec{H}_0 &= \left(\vec{p}\times\vec{R}^0\right)\sqrt{\varepsilon_0/\mu_0}\exp\left(-jk_0\left(\vec{R}^0\cdot\vec{x}\right)\right).\end{aligned}$$

The functions $\vec{E}^T, \vec{H}^T$ are the distributions of tangential components of field intensity vectors along the aperture given the Kirchhoff's approximation.

Taking into account the cone radome shape, we can conclude that the field scattered by the radome "mirror reflection" at points of aperture is significantly less intense than that passed directly through real radome. Thus, in first approximation, we can assume that $\vec{E}_0(x, \vec{R}^0, \vec{p})$, $\vec{H}_0(x, \vec{R}^0, \vec{p})$ is the field at the aperture point x, which is generated by waves propagating along two paths (see Fig. 4): direct propagation wave (path 1) and the wave reflected from the radome inner surface (path 2). The integrals in Eq. (29) were calculated by method of mean rectangles.

So, to calculate the field $\vec{E}_0$, $\vec{H}_0$, we can use the results obtained during modeling scattering characteristics of antenna system (Section 2.1).

We note that antenna polarization (the direction of vector $\vec{E}^T(x)$) was chosen to be aligned with axis Ox' (see Fig. 6), i.e., to be pointing in the direction, for which aperture size is the greatest. We computed the cross-section of radiation pattern by the plane orthogonal to aperture and passing through axis Ox' (unit vector $\vec{p}$ belongs to that plane and it is orthogonal to the direction $\vec{R}^0$).

Additionally, we also note that the plane containing the perfectly absorbing screen is turned together with antenna if the latter is turned on some angle. In the case of small angles of antenna turn (≤ 25 degrees), all assumptions made with regard to the structure of field $\vec{E}_0(x, \vec{R}^0, \vec{p})$, $\vec{H}_0(x, \vec{R}^0, \vec{p})$ remain valid.

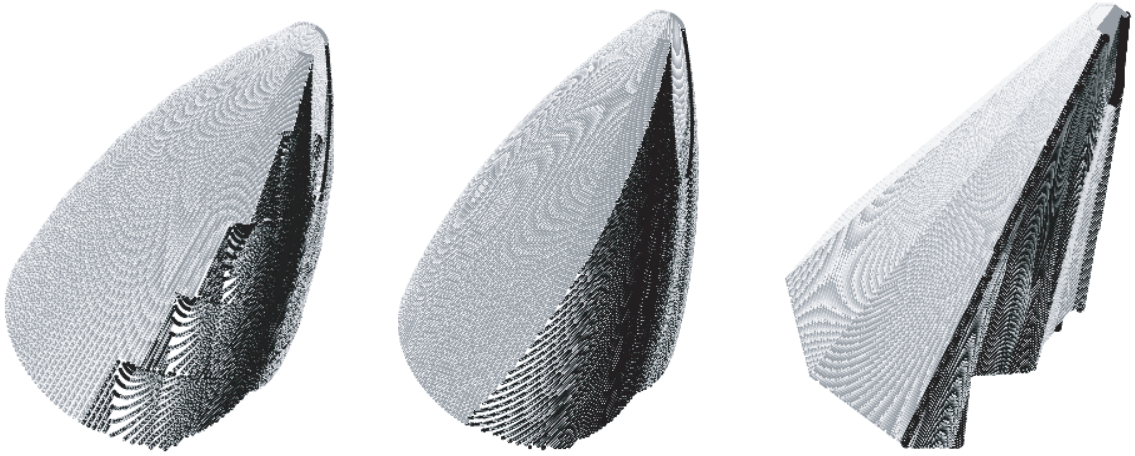

Figure 12. Appearance of "illuminated" and "shadow" zones at the radomes of different kinds: (a) — compound cone; (b) — ogival radome; (c) — pyramidal radome.

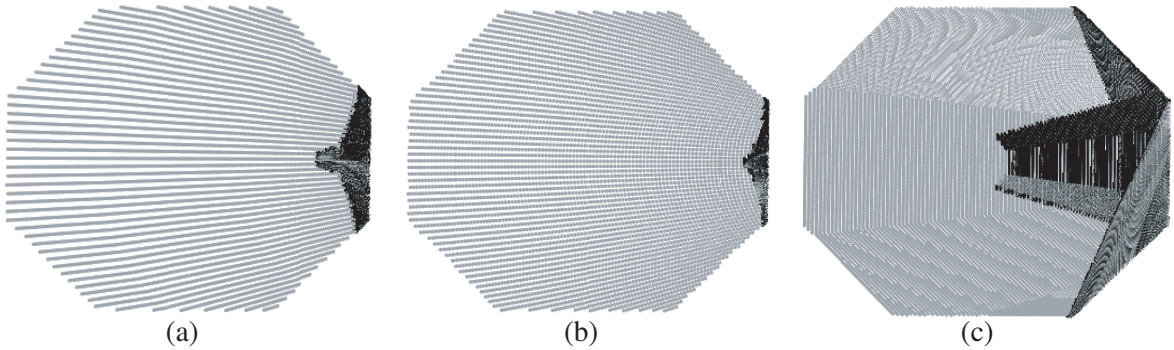

Figure 13. Appearance of zones at the antenna aperture that are illuminated by the wave reflected from the radome "shadow" part given that antenna is under the: (a) — compound cone radome; (b) — ogival radome; (c) — pyramidal radome.

3.2. Results of Numerical Calculation of Radiation from the Antenna System under the Nose Dielectric Radome

As the computation model, we used antenna system with the same parameters and same radome kinds as in Section 2. Operating frequency of antenna was 36.6 GHz (the wavelength was 8.2 mm). The antenna turn angle varied from 0 to 25 degrees.

An example of simulation process of the radiation from antenna system under different kinds of radomes is presented Fig. 12. The figure visualizes the radomes with their "illuminated" (marked as gray) and "shadow" (marked as black) zones. The latter images corresponded to radiation direction of 30 degrees with respect to radome's axis. Further on, appearance of octagonal antenna aperture under different radomes is shown in Fig. 13. Here, the parts of antenna aperture that get illuminated by the field reflected from the radome "shadow" zone are blackened. It should be noted that even presence of wide areas at the antenna that get illuminated by reflected wave (as for pyramidal radome) doesn't lead to significant distortion of antenna radiation pattern.

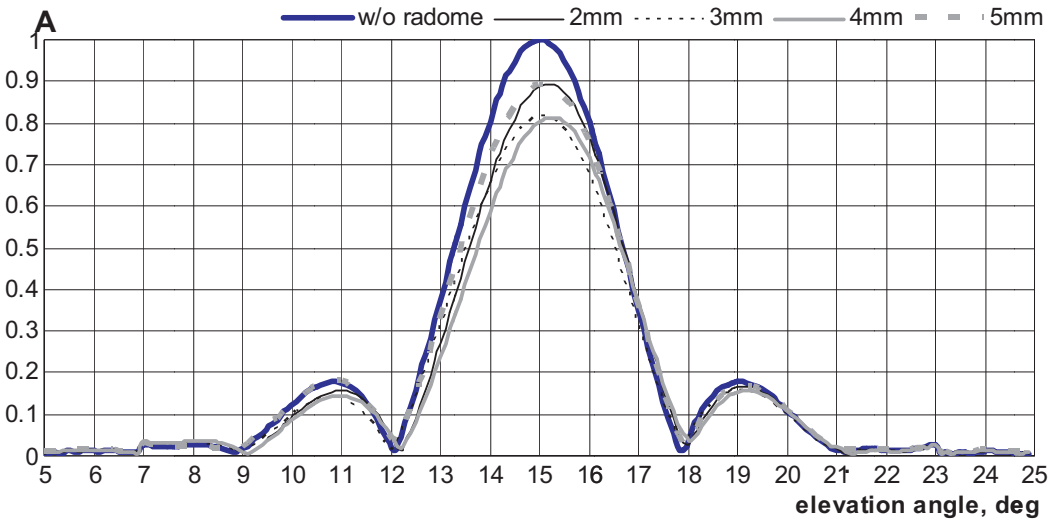

Figure 14. Antenna radiation pattern given different thicknesses of the compound cone radome.

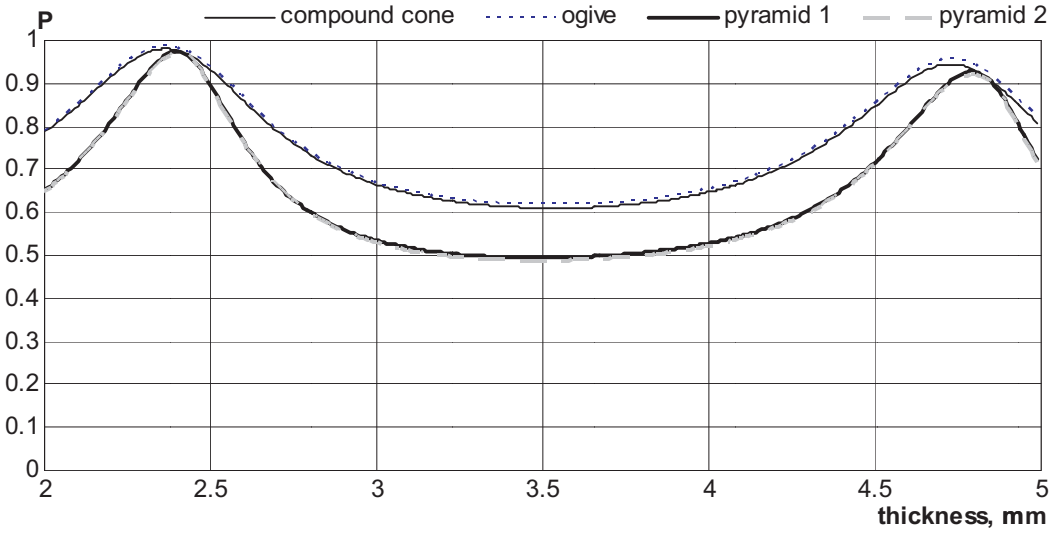

Figure 15. The normalized power radiation pattern maximum versus radome side thickness for different radome kinds given antenna turn angle of 15 degrees.

Figure 14 shows the normalized antenna radiation pattern given different thicknesses of the compound cone radome. The turn angle of antenna aperture was 15 degrees with respect to the radome axis. All patterns were normalized by the maximum of radiation pattern of the antenna without any radome. We can see that the width of pattern main lobe is the same for different thicknesses of radome. The influence of radome manifests itself as a decrease in the maximum of pattern's main lobe. To reduce the radome influence to the antenna power performance, we need to evaluate the optimal thicknesses of radome.

Figure 15 shows the dependencies of the normalized power radiation pattern maxima versus the radome side thickness for different kinds of radome. The antenna turn angle was 15 degrees. The plots corresponding to pyramidal radome include two dependencies differing by orientation of the radiation direction vector: pyramid 1 — radiation direction vector $-\vec{R}_0$ belongs to the plane perpendicular to one of the pyramid sides; pyramid 2 — radiation direction vector $-\vec{R}_0$ belongs to a bisector plane between two radome sides. Results obtained here show that the transmission coefficient has two maxima at the

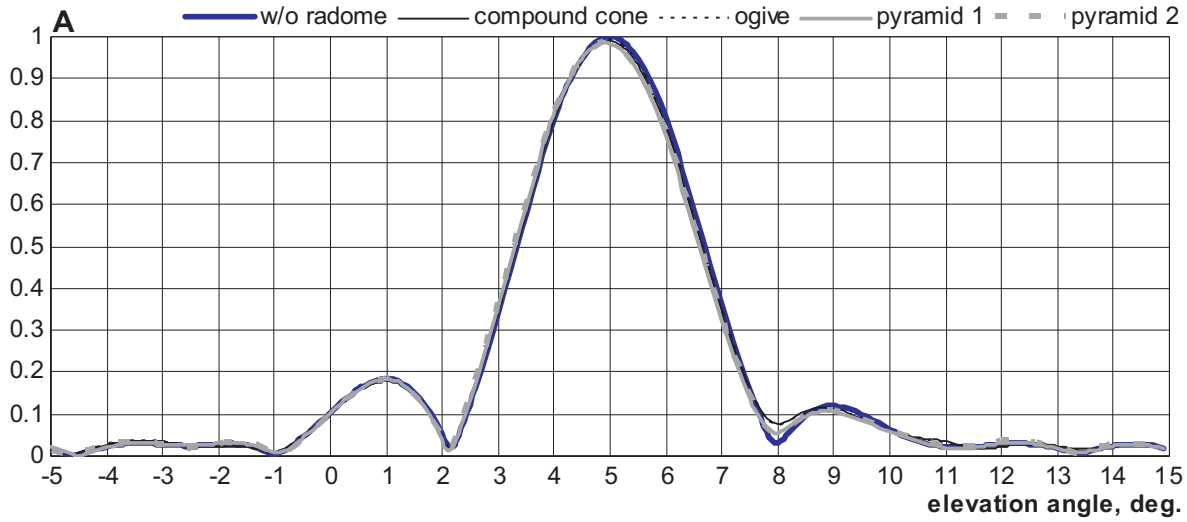

Figure 16. Antenna radiation patterns given antenna turn angle of 5 degrees and radome thickness of 2.4 mm.

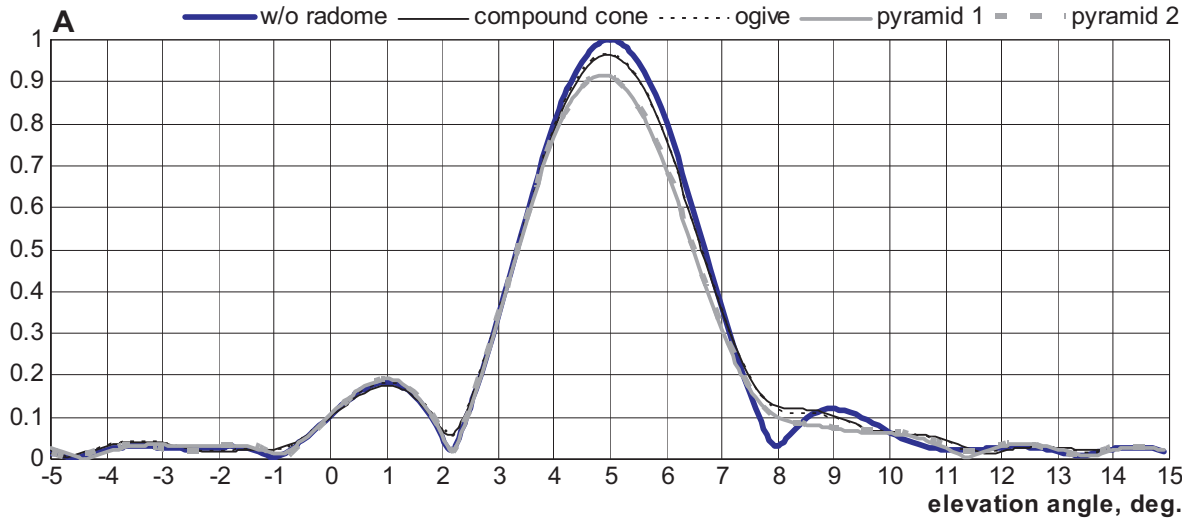

Figure 17. Antenna radiation patterns given antenna turn angle of 5 degrees and radome thickness of 4.75 mm.

radome thickness of 2.4 mm and of 4.75 mm regardless of the radome kind. It should also be noted that positions of maxima are not fixed, as the antenna turn angle varies the maxima shift slightly depending on the radome kind. Thus once the radome kind is selected to house the antenna system, it will be necessary to carry out additional research to accurately evaluate optimal thickness of the radome.

Figures 16–20 show the antenna radiation patterns given different antenna turn angles and optimal radome thicknesses.

Analyses of plots in Figs. 16–21 show that the radiation pattern maxima are practically the same as those for antenna without radome. In the case of radome thickness of 4.75 mm, the decrease in the pattern maxima is more visible than the dependencies obtained given radome thickness of 2.4 mm. This fact is to be accounted for if there is a need to increase the radome thickness. Given the antenna turn angle of 5 degrees, the dips of antenna radiation pattern start to get less pronounced (especially given the radome thickness of 4.75 mm). Given the antenna turn angles of 15–25 degrees, instead of disappearing dips we can notice slight shift in the antenna pattern maximum, which amounts to about 0.1 degree (especially given the radome thickness of 4.75 mm).

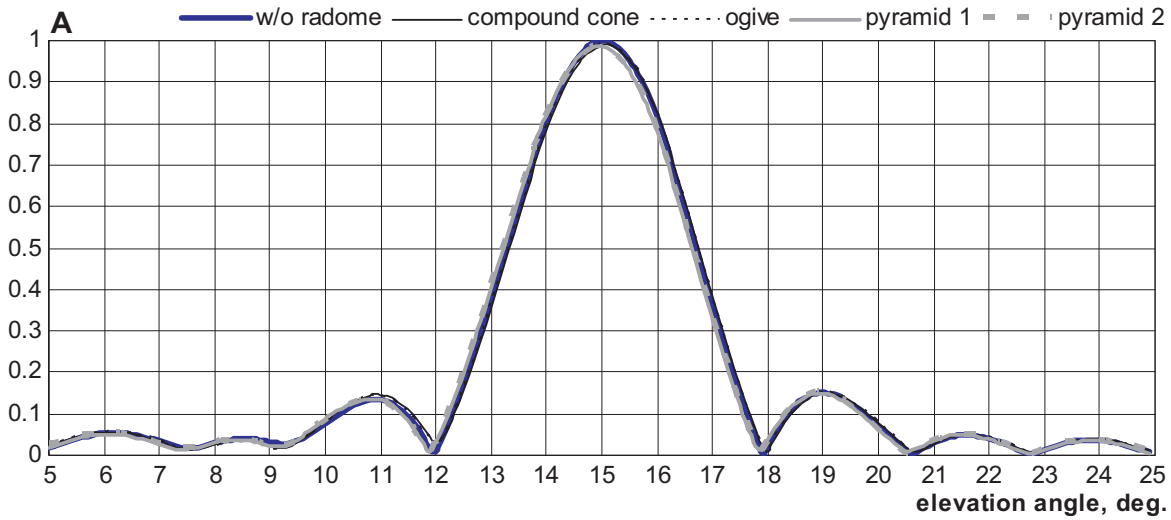

Figure 18. Antenna radiation patterns given antenna turn angle of 15 degrees and radome thickness of 2.4 mm.

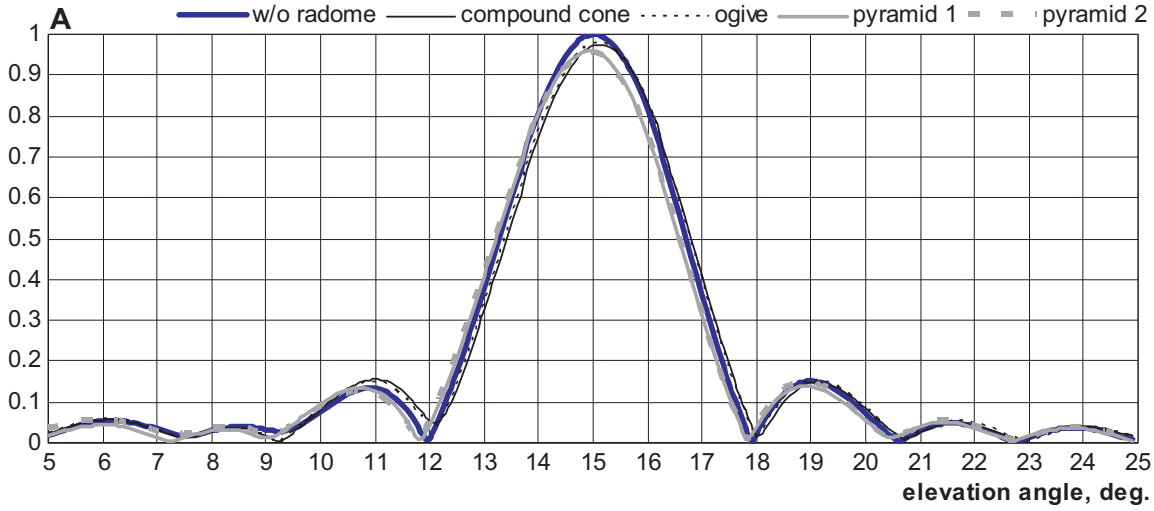

Figure 19. Antenna radiation patterns given antenna turn angle of 15 degrees and radome thickness of 4.75 mm.

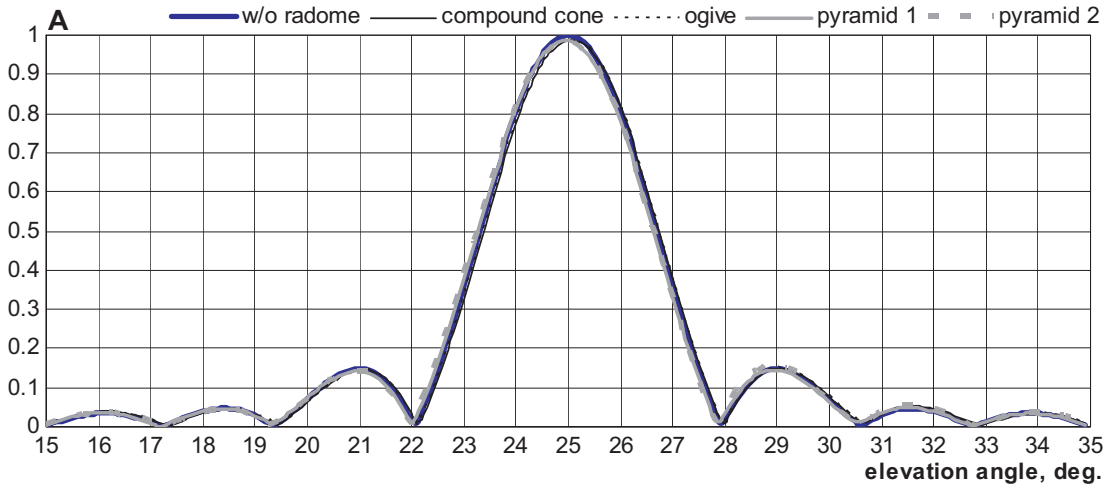

Figure 20. Antenna radiation patterns given antenna turn angle of 25 degrees and radome thickness of 2.4 mm.

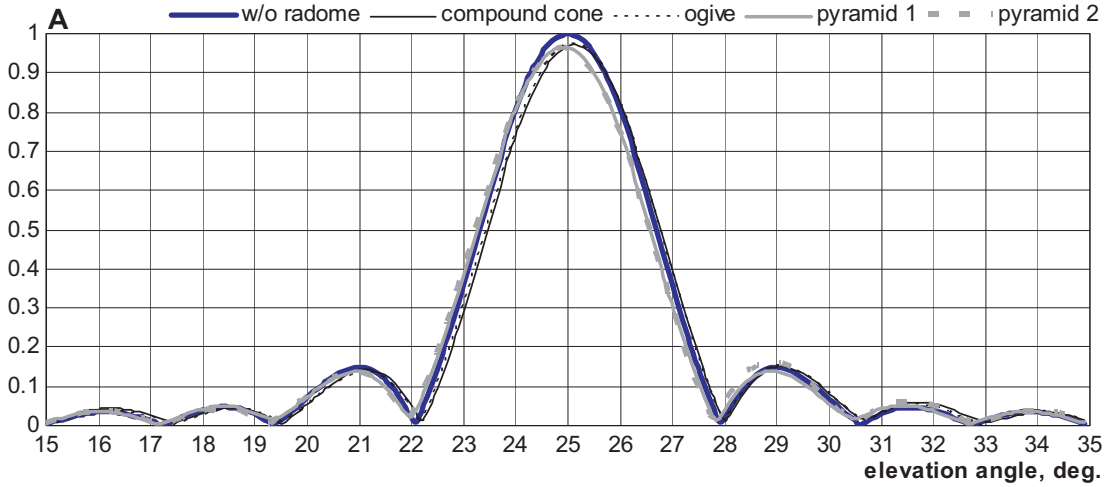

Figure 21. Antenna radiation patterns given antenna turn angle of 25 degrees and radome thickness of 4.75 mm.

4. CONCLUSION

This paper presents the original method for calculating electromagnetic field scattered by the antenna placed inside the nose dielectric radome. Radiation characteristics are obtained using the method for computing the field excited by the radiation aperture given the presence of arbitrary system of scatterers in its vicinity (radome in particular).

The scattering characteristics of antenna system were obtained for the three kinds of nose dielectric radomes: compound cone, ogival, and pyramidal. The RCS of antenna placed in the open (no radome present) given normal incidence of radio wave was 6.60 m^2. Once the antenna was put under radomes of the 2.4 mm and 4.75 mm thicknesses, this maximum decreased down to 2–3 m^2 for parallel polarization of illumination signal and down to 2–4 m^2 for perpendicular polarization of illumination signal. Besides, the pyramidal radome provided slightly better reduction in that maximum as compared to compound cone and ogival radome kinds.

Contribution of metal cap to the RCS of entire antenna system is very small, and its influence onto overall scattering level can be neglected. The main lobe width of the antenna system scattering pattern is less than a few degrees, and its main radiation is concentrated in a narrow sector about direction that

is perpendicular to the antenna aperture. For majority of sounding aspect angles, the RCS of antenna system considered here is less than $0.1\,m^2$ regardless of radome kind.

The radiation characteristics of antenna system under radome were estimated given different parameters of system. The radome use can affect the radiation pattern of antenna system. Its influence manifests itself in reduced power of the radiation pattern main lobe, in changes in its width, in disappearing dips of radiation pattern, and in slight shifts of the radiation pattern maximum of about 0.1 degree.

Using the results of calculations, we figured that "optimal" radome thicknesses is equal to 2.4 mm and 4.75 mm given the antenna operating frequency of 36.6 GHz. Radiation pattern maxima are almost the same as those for antenna without radome given that radome of such thickness is to be employed. Given the antenna turn angle of 5 degrees, the dips of antenna radiation pattern start to fill in. Given the antenna turn angles of 15–25 degrees, there is slight shift in the antenna pattern maximum amounting to 0.1 degree.

REFERENCES

1. Kozakoff, D. J., *Analysis of Radome-Enclosed Antennas*, 2nd Edition, 294, Artech House, Inc., 2010.
2. Kaplun, V. A., "Radomes of microwave antennas," *Sovetskoe Radio*, Moscow, 1974 (in Russian).
3. Kaplun, V. A. and V. M. Zelenkevich, "Introduction to computer-aided design of microwave antenna radomes," *Radiotechnika i Electronika (USSR)*, Vol. 42, No. 2, 89–93, 1987 (in Russian).
4. Zamyatin, V. I. and O. I. Sukharevsky, "The backscattering of reflector antenna with dielectric envelope from side source waves," *Antenny, Issure 37, Radio I Svyaz*, 78–87, 1990 (in Russian).
5. Mikhailov, G. D., S. N. Kutischev, and O. E. Kiryanov, "Radar cross-section of reflector antenna with dielectric radome," *Izvestiya vuzov. Radiophysika*, Issue XLII, 879–885, 1999 (in Russian).
6. Lansink Rotgerink, J., H. van der Ven, T. Voigt, E. Jehamy, M. Schick, and H. Schippers, "Modelling of effects of nose radomes on radar antenna performance," *10th European Conference on Antennas and Propagation (EuCAP)*, 1–5, 2016.
7. Liu, S., H. Zhou, C. Ding, and L. Song, "Electrical properties analysis of conical radome," *2016 IEEE International Conference on Ubiquitous Wireless Broadband (ICUWB)*, 1–4, 2016.
8. Mrdakovic, B. L. and B. M. Kolundzija, "A method for full wave analysis of electrically large transparent radomes," *2016 IEEE International Symposium on Antennas and Propagation (APSURSI)*, 1331–1332, 2016.
9. Sheret, T., C. Parini, and B. Allen, "Efficient design of a radome for minimized transmission loss," *IET Microwaves, Antennas & Propagation*, Vol. 10, No. 15, 1662–1666, 2016.
10. Rim, J.-W., I.-S. Koh, and K. S. Choi, "IPO analysis of performance of arbitrary shaped radome," *10th European Conference on Antennas and Propagation (EuCAP)*, 1–5, 2016.
11. Nair, R. U., M. Suprava, and R. M. Jha, "Graded dielectric inhomogeneous streamlined radome for airborne applications," *Electronics Letters*, Vol. 51, No. 11, 862–863, 2015.
12. Kim, J. H., Y. B. Park, and S.-C. Song, "Electromagnetic analysis of a tangent-ogive dielectric radome with a metallic cap," *2015 International Workshop on Antenna Technology (iWAT)*, 367–368, 2016.
13. Dwivedi, S. and V. Mishra, "Numerical analysis for directivity improvement of radome structure," *2013 IEEE Applied Electromagnetics Conference (AEMC)*, 1–2, 2013.
14. Borovikov, V. A. and B. Y. Kinber, *Geometrical Theory of Diffraction*, IEE, UK, 1994.
15. Sukharevsky, I. V. and S. E. Vashinski, "About the stationary phase points and caustic influence on lateral radiation of antenna systems with radomes," *MMET-98, Conference Proceedings*, Vol. 2, 537–539, Kharkov, 1998.
16. Sukharevsky, O. I., et al., *Electromagnetic Wave Scattering by Aerial and Ground Radar Objects*, 332, O. I. Sukharevsky (ed.), CRC Press, 2014.
17. Rosloniec, S., *Fundamental Numerical Methods for Electrical Engineering*, Springer Science & Business Media, 2008.